inorganics

MDPI

Article

Hierarchically Porous Titanosilicate Hollow Spheres Containing TS-1 Zeolite Precursors for Oxidative Desulfurization

Yao Wang, Hongda Yu, Huan Wang and Tiehong Chen *

Smart Sensing Interdisciplinary Science Center, Institute of New Catalytic Materials Science, School of Materials Science and Engineering, Nankai University & Cangzhou Bohai New Area Green Chemical Institute, Nankai University, Tianjin 300350, China

* Correspondence: chenth@nankai.edu.cn

Abstract: The environmental and health impacts of sulfur compounds in fuel oil have prompted considerable research interest in oxidative desulfurization (ODS) technology. Tetrahedrally coordinated titanium has been demonstrated to exhibit excellent activity in the context of oxidative desulfurization processes. However, further improving the catalytic property of the tetrahedrally coordinated titanium remains a challenging endeavor. In the context of ODS processes conducted at near room temperatures, the improvement of conversion remains a subject of considerable challenge. In this study, hierarchically porous titanosilicate hollow spheres were synthesized by using TS-1 zeolite precursors as Ti and Si sources to obtain the catalyst with only tetrahedrally coordinated titanium. The synthesized materials were characterized through transmission electron microscopy (TEM), Fourier-transform infrared spectroscopy (FT-IR), ultraviolet–visible diffuse reflectance spectroscopy (UV-Vis), and nitrogen adsorption analysis. These techniques confirmed the formation of hollow spherical hierarchically porous structures with Ti species uniformly incorporated in tetrahedral coordination and the presence of five-member rings of TS-1 zeolite. As a result, the hierarchically porous titanosilicate hollow spheres demonstrated excellent catalytic performance in ODS, achieving complete dibenzothiophene (DBT) removal within 15 min and a high turnover frequency (TOF) of up to 123 h^{-1} at 30 °C.

Keywords: hierarchically porous; titanosilicate; hollow spheres; oxidative desulfurization

Academic Editors: Torben R. Jensen and Roberto Nisticò

Received: 19 December 2024
Revised: 21 January 2025
Accepted: 22 January 2025
Published: 25 January 2025

Citation: Wang, Y.; Yu, H.; Wang, H.; Chen, T. Hierarchically Porous Titanosilicate Hollow Spheres Containing TS-1 Zeolite Precursors for Oxidative Desulfurization. *Inorganics* **2025**, *13*, 37. https://doi.org/10.3390/inorganics13020037

1. Introduction

Fuel oil is widely utilized as energy source; however, its high quantity of sulfur remains a problem that needs to be solved [1]. During the combustion of gasoline and diesel, sulfur compounds such as dibenzothiophene (DBT), 4,6-dimethyldibenzothiophene (4,6-DMDBT), and 4-methylbenzothiophene (4-MDBT) produce sulfur oxides, which are harmful to human health and contribute to environmental pollution [2]. In response, stricter sulfur content regulations have been introduced worldwide, attracting research interest for development of effective petroleum desulfurization technologies [3–6]. Despite the recent advancements in the field, the efficient removal of sulfur compounds from fuel oils using minute quantities of catalysts at ambient temperatures is still rare.

Hydrodesulfurization (HDS) is the most prevalent industrial technology utilized for sulfur removal due to its high efficiency [7]. However, producing ultra-low sulfur fuels

with HDS requires high temperatures, high pressures, and significant hydrogen consumption, which increases operational costs and complicates process control [8]. To overcome these limitations, alternative non-hydrodesulfurization methods, such as biological desulfurization [9], adsorption desulfurization [10,11], extraction desulfurization [12], and oxidative desulfurization (ODS) [13] have been explored. Among them, ODS eliminates the need for hydrogen, enhancing operational safety and reducing costs. The two types of ODS are non-catalytic and catalytic; while non-catalytic ODS is compatible with oils that contain high levels of sulfur, it necessitates elevated reaction temperatures and extended reaction times [14]. In contrast, catalytic ODS has emerged as particularly promising, as it efficiently removes sulfur compounds under mild conditions, including ambient pressure and reaction temperatures below 100 °C [15]. More importantly, aromatic sulfur-containing organic compounds (ASOCs) including DBT, 4,6-DMDBT, and 4-MDBT are not easily eliminated through the HDS process because of steric hindrance; in contrast, ASOCs can be efficiently removed through the ODS process under mild conditions [16].

The ODS process means that sulfur compounds are catalytically oxidized into more polar sulfone derivatives, which can then be separated from hydrocarbons through adsorption or extraction [17]. The most common oxidants are hydrogen peroxide (H_2O_2) and tert-butyl hydroperoxide (TBHP). H_2O_2 is often favored for its environmental friendliness and cost-effectiveness; however, the reaction occurs in a biphasic water/oil system. In this setup, sulfur compounds remain in the oil phase, while the catalyst and H_2O_2 are in the aqueous phase, causing mass transfer limitations that hinder the oxidation rate [18]. In comparison, TBHP, being oil-soluble, enables the reaction to proceed in a single-phase system, eliminating interfacial mass transfer limitations and enhancing reaction performance [19–21].

Various catalysts have shown significant potential in oxidative desulfurization (ODS), including transition metal oxides [22,23], TS-1 zeolite [24,25], and mesoporous silica [26,27]. Careo et al. [23] investigated ODS reactions in synthetic diesel using vanadium oxide catalysts supported on titanium, analyzing the impact of operating conditions on sulfur removal efficiency. Similarly, Du et al. [24] synthesized hierarchical porous TS-1 (HTS) using a soft-template method. The hierarchical pore structure of HTS enabled superior dibenzothiophene (DBT) removal compared to conventional TS-1, which relies solely on microporous structures and demonstrated lower efficiency under identical conditions. Furthermore, the use of mesoporous materials has been shown to enhance ODS performance due to their large pore channels, which improve the accessibility of sulfur compounds. For instance, Cho et al. [28] synthesized Ti-SBA-15 through a grafting method, achieving good catalytic activity [29,30]. In summary, some ODS catalysts have been reported; however, their activities remain unsatisfactory and introduce single tetrahedrally coordinated Ti to the catalysts, which is still a challenge.

Previous studies [31,32] have demonstrated that aging a solution containing appropriate amounts of silicon sources and template agents, such as TPAOH or TEAOH, at controlled temperatures produces a transparent solution rich in zeolite primary and secondary structural units, along with nanoclusters formed through their aggregation. Adding Ti species to the above precursors makes it more likely that material precursors containing tetrahedrally coordinated Ti will be obtained. In addition, due to their substantial surface area and comparatively short channels, which are conducive to molecular diffusion, hierarchically porous nanoparticles are frequently used as catalytic support and a variety of templates have been shown to facilitate the synthesis of hierarchically porous structures such as PEO-*b*-PMMA and CTAB [33], P123 and SDS [34], and CTAB-PAA [26,35].

Herein, hierarchically porous titanosilicate hollow spheres (Ti-HHS) containing TS-1 zeolite precursors were synthesized using a polyelectrolyte–surfactant mesoporous complex template as a structure-directing agent. Ti-HHS exhibited hollow spherical mesoporous structures with Ti species uniformly incorporated in tetrahedral coordination and the presence of five-member rings of TS-1 zeolite, and gave rise to excellent catalytic performance in ODS, achieving complete dibenzothiophene (DBT) removal with a high turnover frequency (TOF) of up to 123 h^{-1} at 30 °C.

2. Results and Discussion

2.1. Characterization of Ti-HHS

The synthesis of the Ti-HHS mechanism is outlined in Figure 1. The small-angle XRD patterns of the calcined Ti-HHS-1, Ti-HHS-2, and Ti-HHS-3 samples are presented in Figure 2a. These patterns display a single broad diffraction peak around 2.0°, consistent with the worm-like pore structures observed in the TEM images. Figure 2b shows the wide-angle XRD patterns of the same samples. A broad diffraction peak centered at 23° is observed, corresponding to the characteristic peak of amorphous silica. No diffraction peaks associated with zeolite crystal structures or titanium species are detected.

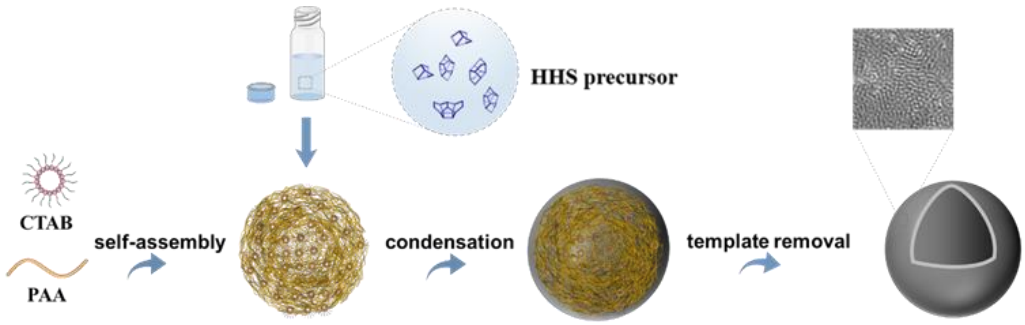

Figure 1. Schematic representation of the synthesis mechanism of hierarchically porous titanosilica hollow spheres.

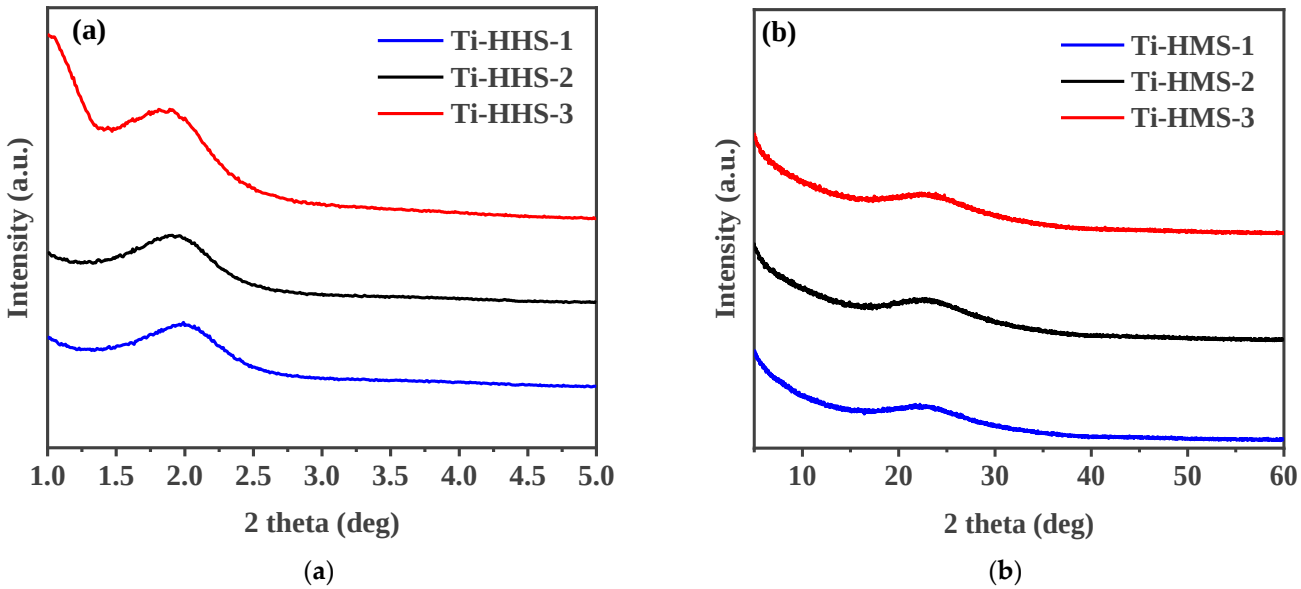

Figure 2. Small-angle XRD patterns (**a**) and wide-angle XRD patterns (**b**) of hierarchically porous titanosilicate hollow spheres with various Ti contents: Ti–HHS–1, Ti–HHS–2, and Ti–HHS–3.

The SEM and TEM images of Ti-HHS-3 are shown in Figures 3 and 4, respectively. The SEM images (Figure 3) reveal that Ti-HHS-3 has a uniform spherical morphology with particle sizes ranging around several hundreds of nanometers and exhibits good particle dispersion. Figure 3b shows a rough particle surface with visible macropores. The TEM images in Figure 4a confirm that the hollow spherical shell structure is consistent across the sample, supporting the observations from the SEM images. Figure 4b indicates that the shell thickness ranges from 20 to 40 nanometers. Figure 4d, an enlarged view of Figure 4c, highlights the uniformly distributed wormhole structure within the particles, further emphasizing the hierarchical porous characteristics of the sample [36,37].

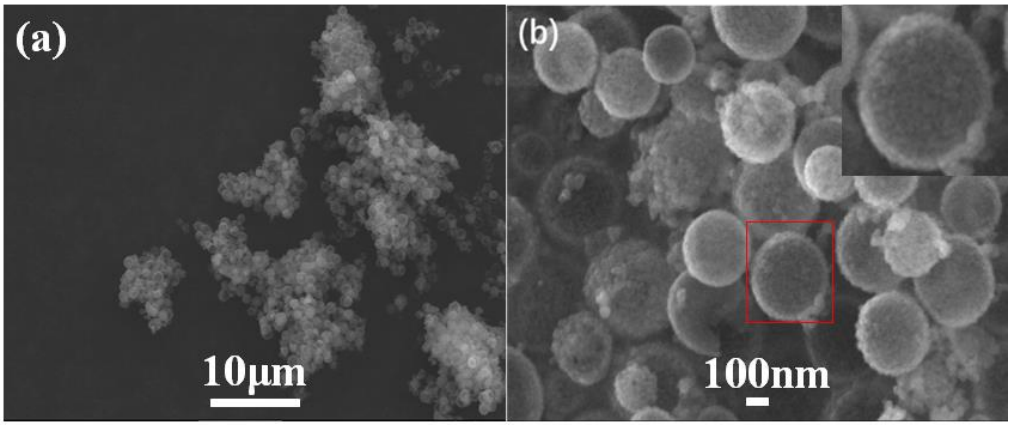

Figure 3. SEM images of Ti−HHS−3. (**a**) ×2000, and (**b**) ×50,000, the red square indicates the original location of the enlarged image, which is situated in the upper right corner.

The EDS mapping for Ti-HHS-3, presented in Figure 5, characterizes the Ti distribution within the sample. The mapping confirms a uniform distribution of Ti throughout the hollow sphere structure, with no evidence of local aggregation or clustering. These results validate the successful incorporation of Ti into all three samples. The titanium content in the sample was determined by ICP-AES; the Ti content of Ti-HHS-1, Ti-HHS-2, and Ti-HHS-3 are 0.55 wt%,1.46 wt%, and 2.60 wt%, respectively.

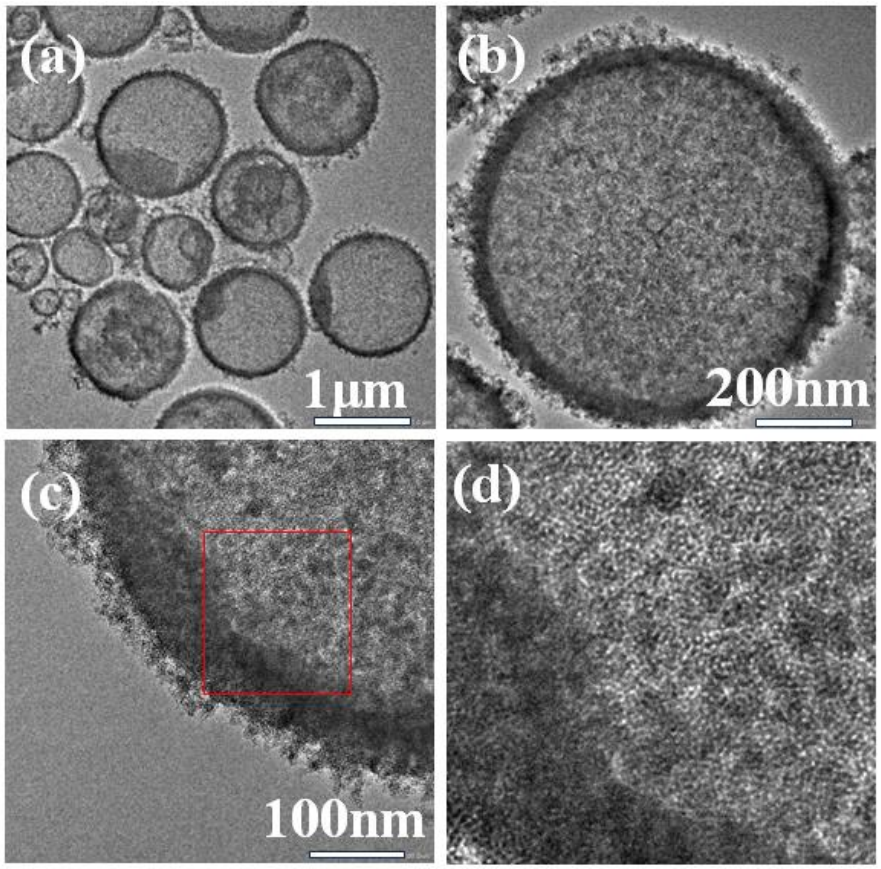

Figure 4. TEM images of Ti−HHS−3. (**a**)1 μm, (**b**)200nm, (**c**)100nm, and(**d**)enlarged view of the red square in figure (**c**).

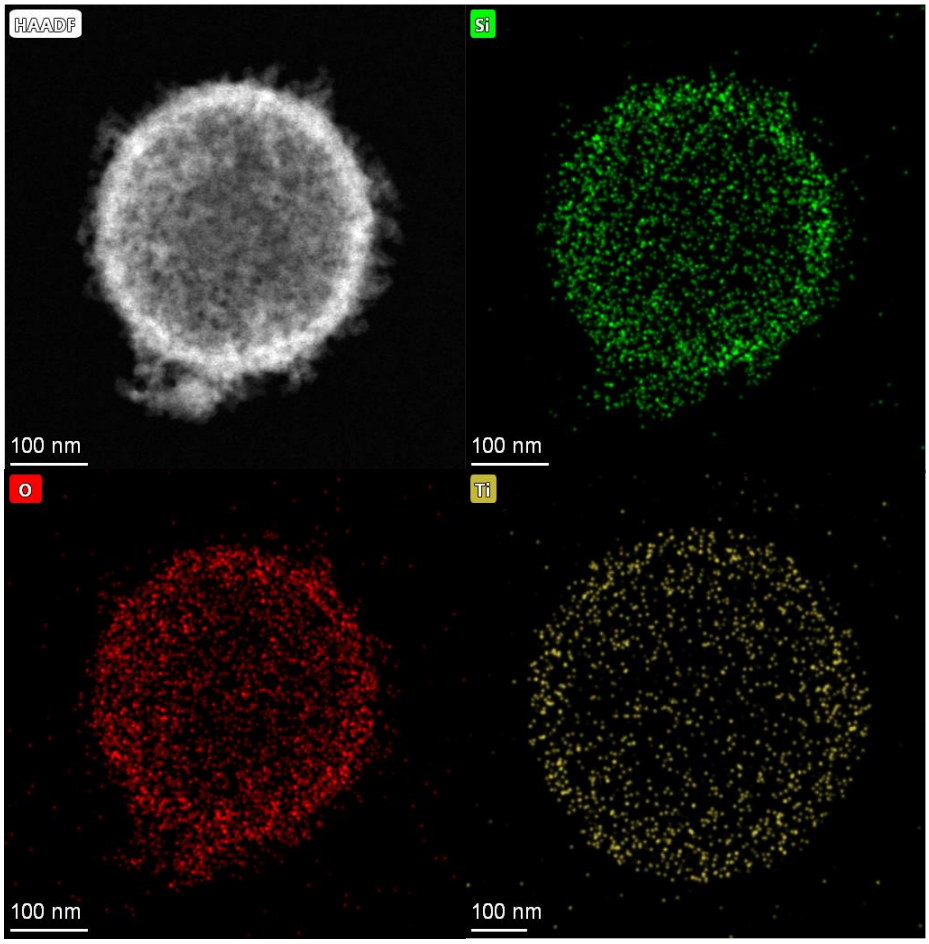

Figure 5. EDS–mapping images of Ti–HHS–3.

Figure 6a,b present the nitrogen adsorption–desorption isotherms and the corresponding pore size distribution curves for the hierarchically porous titanosilicate hollow sphere samples. All three samples exhibit typical Type IV isotherms with an H3-type hysteresis loop, characterized by two adsorption steps in the relative pressure (P/P_0) range of 0.25–0.35 and 0.85–0.95 in Figure 6a. The first step corresponds to a peak at approximately 3 nm in Figure 6b, indicating the presence of wormhole-like mesopores within the samples [36,37]. The second step corresponds to the larger pores within the shell template by phase-separated PAA [35]. Furthermore, the nearly overlapping adsorption–desorption curves suggest highly accessible mesopores, consistent with the thin-shell structure of the hollow spheres. According to Table 1, the three samples show relatively large specific surface areas and pore volumes. While the surface area and pore volume of Ti-HHS-3 are lower than Ti-HHS-1 and Ti-HHS-2, which probably owes to different additions of Ti species [38].

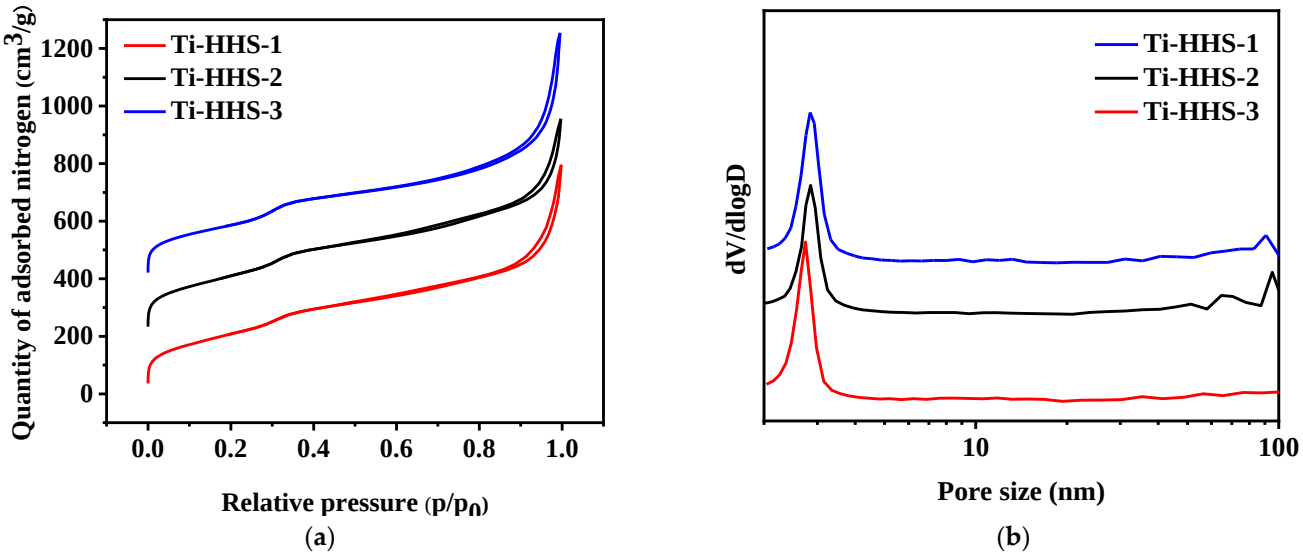

Figure 6. Nitrogen adsorption–desorption isotherms (**a**) and pore size distribution curves (**b**) for Ti–HHS–1, Ti–HHS–2, and Ti–HHS–3.

Table 1. The detailed structural parameters of the samples.

Samples	Mesopore Size (nm)	S_{BET} (m^2/g)	V_{MIC} (cm^3/g)	V_{MES} (cm^3/g)
Ti-HHS-1	2.8	710	0.005	1.022
Ti-HHS-2	2.8	647	0.006	0.915
Ti-HHS-3	2.8	600	0.009	0.941

As shown in the FT-IR spectra in Figure 7, all three samples exhibit characteristic absorption peaks at 810 cm^{-1} and 1053 cm^{-1}. These absorption peaks correspond to the symmetric and asymmetric Si–O–Si stretching vibrations, respectively, which are typical features of amorphous silica in infrared spectra [39]. Additionally, a minor absorption peak appears at 560 cm^{-1} in the Ti-HHS-1, Ti-HHS-2, and Ti-HHS-3 samples. This peak is associated with the stretching vibrations of double five-membered rings in MFI structures [40], suggesting the presence of primary and secondary zeolite structural units and indicating short-range order within the samples. Each sample also shows a distinct absorption peak at 960 cm^{-1}, attributed to Si–O–Ti vibrations [39,41], confirming the incorporation of Ti into the structure. Furthermore, the intensity of the 960 cm^{-1} peak decreases with lower Ti content, particularly in the Ti-HHS-1 sample, where the peak at 960 cm^{-1} is less prominent.

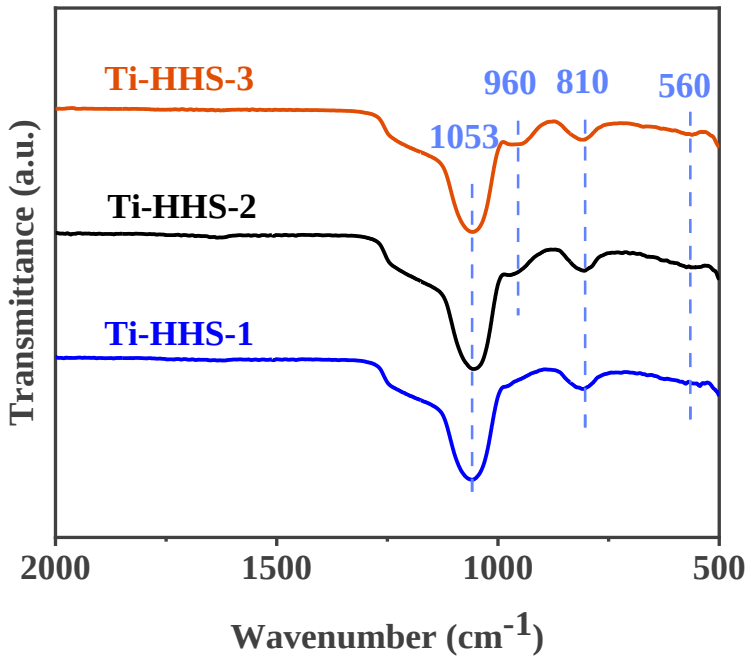

Figure 7. FT−IR spectra for the Ti−HHS−1, Ti−HHS−2, and Ti−HHS−3.

UV−visible absorption spectroscopy was employed to investigate the coordination state of Ti species in the hierarchically porous titanosilicate hollow spheres. As shown in Figure 8, all three samples exhibit a narrow, strong absorption peak at 215 nm, with no additional peaks observed at longer wavelengths. The absorption peak near 220 nm is characteristic of the tetrahedral coordination of Ti species within the framework [42]. These results confirm that the doped Ti exists exclusively in tetrahedral coordination within the framework, with no evidence of non-framework octahedral Ti species or separate crystalline TiO_2 phases [43,44].

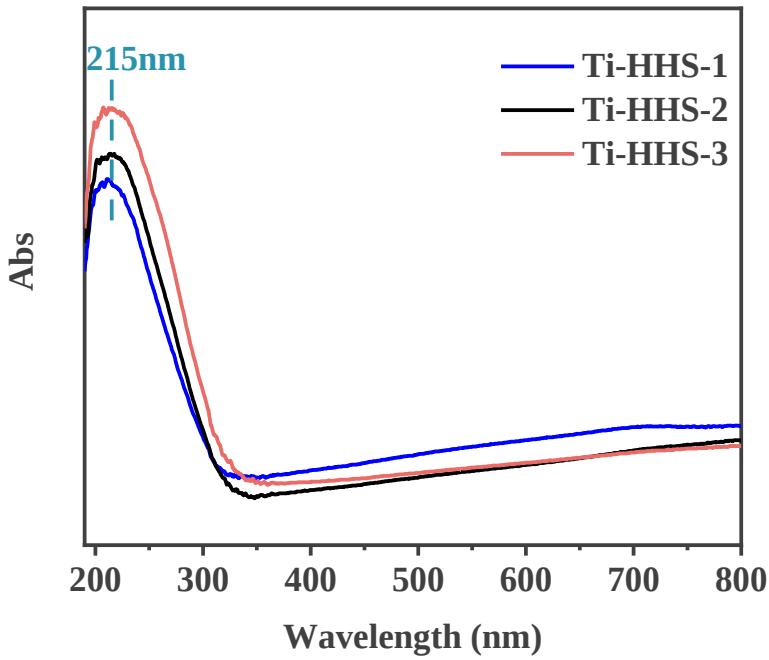

Figure 8. UV−vis spectra for the Ti−HHS−1, Ti−HHS−2, and Ti−HHS−3.

2.2. ODS Performance of Ti-HHS

In the ODS reaction at 30 °C, both the catalyst and oxidant are crucial for effective desulfurization. As shown in Figure 9a, the sulfur compound conversion rate remains low in the absence of an oxidant, and no significant conversion occurs without a catalyst. However, the simultaneous introduction of the Ti-HHS-3 catalyst and the oxidant (TBHP) results in rapid DBT conversion, reaching 100% within 15 min. Previous studies [32,45] have demonstrated that tetrahedral Ti sites exhibit higher oxidation activity compared to Ti species in amorphous silica. Structural characterization of Ti-HHS-3 confirms the presence of Ti species primarily in tetrahedral coordination, which significantly enhances its activity. As illustrated in Figure 9b, the Ti-HHS-3 catalyst, synthesized from TS-1 precursor, exhibits substantially higher ODS activity than TiO_2/HHS prepared via direct the impregnation of TiO_2 with an equivalent Si/Ti molar ratio. The catalytic ODS process is shown in Figure 10, and, as reported in the literature, sulfoxides exhibited a high polarity and tended to be absorbed onto the silanol groups in silica via hydrogen bonding, achieving a one-pot oxidation−adsorption process with the hierarchically porous titanosilicate [26].

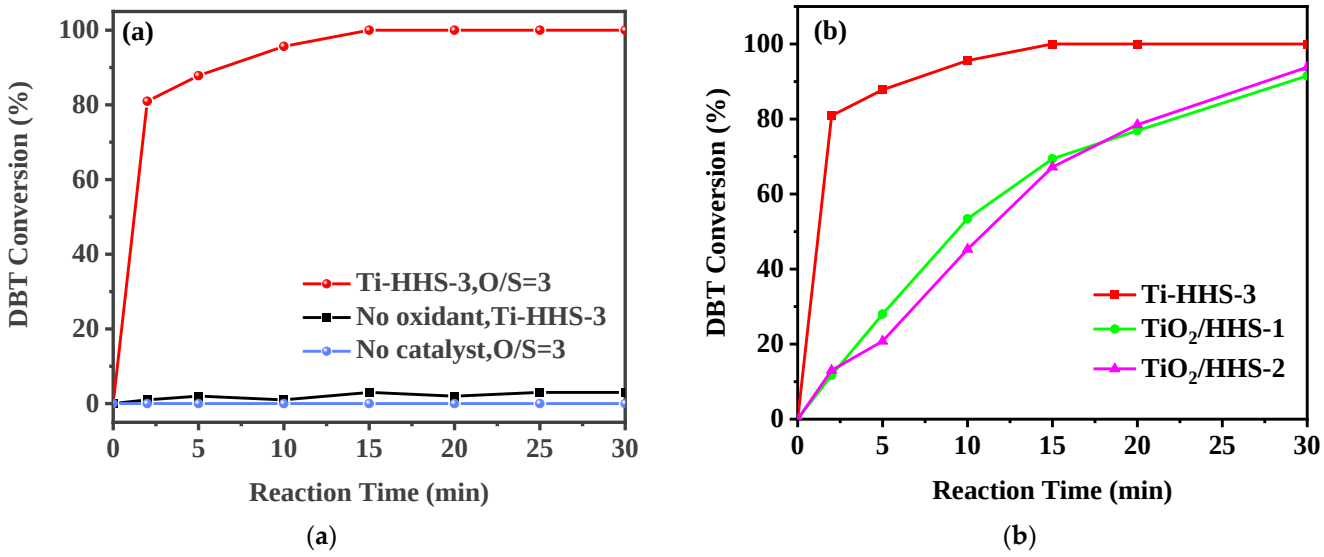

Figure 9. (**a**) DBT ODS activity of the titanosilicate hollow spheres under various conditions. (**b**) Comparison with impregnated catalysts Ti/HHS−1 and Ti/HHS−2 (reaction conditions: 20 g of 500 ppm model gasoline, 20 mg catalyst, 30 °C, O/S = 3).

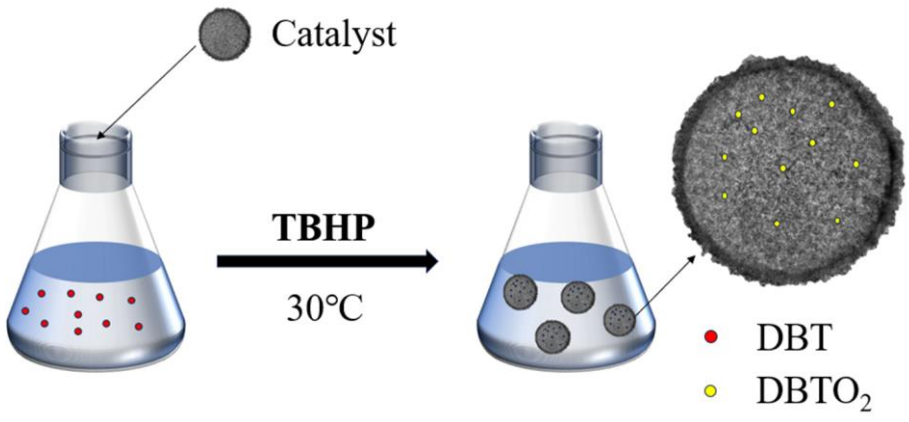

Figure 10. The flow chart of the ODS process.

The ODS activity of catalysts with varying Ti content (Ti-HHS-1, Ti-HHS-2, and Ti-HHS-3) was evaluated under identical conditions. As shown in Figure 11, Ti-HHS-3 exhibits the highest catalytic performance, achieving 100% DBT conversion within 15 min. In contrast, Ti-HHS-1 and Ti-HHS-2 achieve only 71% and 94% conversion after 30 min, respectively. These results highlight the critical role of Ti content in enhancing catalytic activity. At the 2 min mark, Ti-HHS-3 achieves a TOF of up to 123 h^{-1}, which could be due to the tetrahedrally coordinated Ti of the TS-1 precursors in Ti-HHS-3. As illustrated in Table 2, an analysis of the extant literature reveals a range of catalysts with different levels of performance in the oxidation of DBT. It is evident that Ti-HHS-3 exhibits higher activity than the majority of reported catalysts, especially the TOF, although it should be noted that Ti-HHS-3 operates at near room temperature.

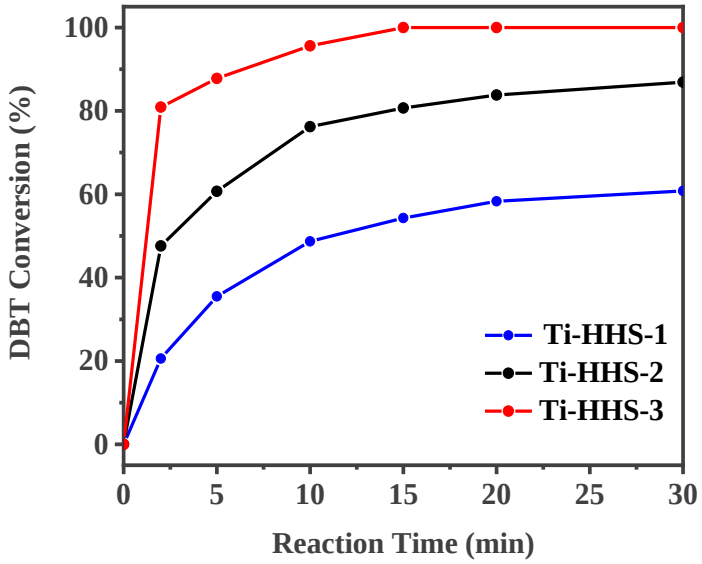

Figure 11. DBT ODS activity of Titanosilicate hierarchically porous hollow spheres with varying Ti content (reaction conditions: 20 g of 500 ppm model gasoline, 20 mg).

Table 2. Comparison of catalytic ODS performance of DBT with different catalysts.

Catalysts	Ti Content (wt%)	S Content (ppm)	Oxidant	Temperature (°C)	TOF (h^{-1})	Ref.
Ti-HHS-3	2.6	500	TBHP	30	123	This work
Ti-B-M-DA	5.5	1000	TBHP	60	58.8	[46]
Ti-SBA-2	5.5	500	TBHP	40	48.8	[47]
Meso-TS-1	0.98	174	H_2O_2	60	3.7	[48]
NSTS-10	2.7	500	TBHP	25	14.9	[26]
Ti-HMS	0.88	584	H_2O_2	70	1.8	[49]
Ti-MCM-41S	1.26	1740	TBHP	80	18.2	[19]

As shown in Figure 12, with an O/S ratio of 1, the DBT conversion rate reaches 95.51% within 30 min, but complete conversion is not achieved. A closer examination of the conversion rate over time reveals a plateau after 15 min, indicating that this ratio is insufficient for full DBT conversion. When the O/S ratio is increased to 3, DBT conversion reaches 100% within 15 min. With further increases in the oxidant ratio to 6 and 9, the conversion of DBT did not change too much. These findings suggest that an optimal O/S ratio exists for efficient DBT conversion while minimizing oxidant consumption. Accordingly, an O/S ratio of 3 is identified as optimal, and all subsequent investigations in this study are based

on this ratio. It was reported that octane could not be oxidized by TBHP below 80 °C [50]; thus, in our experiments, the oxidation of model oil by TBHP could be neglected.

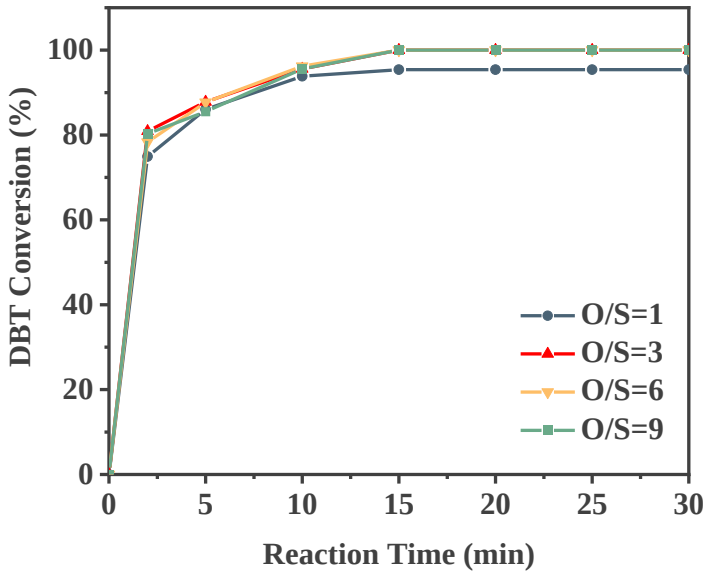

Figure 12. Effect of O/S molar ratio on ODS reaction (reaction conditions: 20 g of 500 ppm model gasoline, 20 mg Ti-HHS-3 catalyst, 30 °C).

In industrial applications, the concentration of sulfur compounds in fuel oil can vary significantly. To more accurately simulate the sulfur concentrations found in actual fuel oils, Ti-HHS-3 was selected as the catalyst to conduct the ODS reaction on model gasolines with different sulfur contents. The model gasolines were prepared with sulfur concentrations of 500 ppm, 1000 ppm, and 2000 ppm, as shown in Figure 13. As the DBT concentration increased, the conversion rate of the sulfur compounds significantly decreased over the same period. Notably, when the DBT concentration reached 2000 ppm, complete conversion could not be achieved within 30 min. This may be attributed to the relatively low Ti doping in Ti-HHS-3, resulting in insufficient catalytic active sites to meet the demands of the reaction at high concentrations, thereby causing a significant decline in catalytic activity.

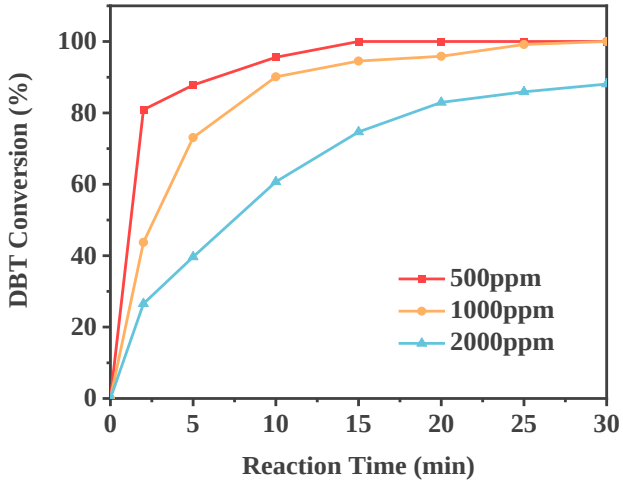

Figure 13. Conversion of different DBT concentrations over Ti−HHS−3 (reaction conditions: 20 g of model gasoline, 20 mg catalyst, 30 °C, O/S = 3).

The reaction temperature is one of the critical parameters influencing catalyst activity. As shown in Figure 14, complete DBT conversion requires 15 min at 30 °C. When the reaction temperature is increased to 50 °C, the time for complete DBT conversion decreases to 10 min. Further increasing the temperature to 80 °C reduces the conversion time to just 2 min. These results demonstrate that the ODS reaction catalyzed by Ti-HHS-3 is highly temperature-dependent, with reaction rates significantly increasing at higher temperatures. As the reaction temperature increases, the conversion efficiency of sulfur compounds improves, highlighting the potential for temperature optimization in practical applications. Higher temperatures likely enhance the reactivity of the catalyst's active sites, reducing the activation energy and thereby accelerating the reaction.

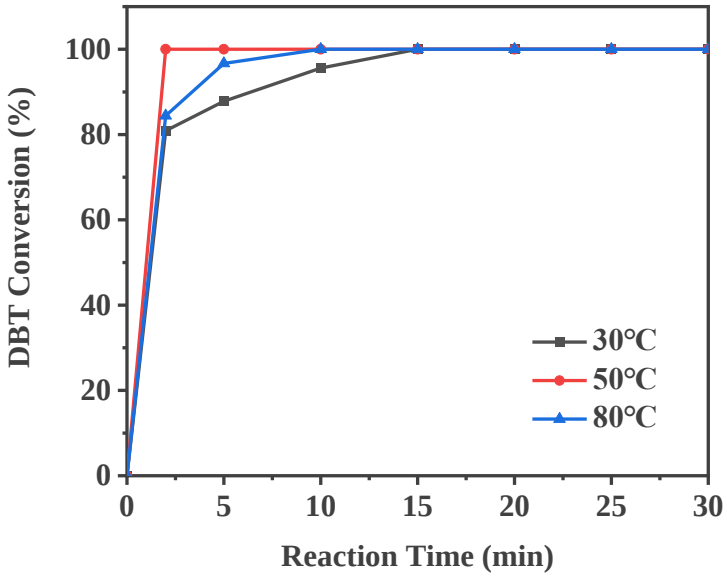

Figure 14. Effect of reaction temperature on DBT conversion (Reaction conditions: 20 g of 500ppm model gasoline, 20 mg catalyst, O/S = 3).

Fuel oils commonly used in daily life include petrol and diesel. Compared to gasoline, diesel contains longer alkane chains and boils in the range of 180–350 °C. To model diesel fuel, this study used long-chain alkanes, specifically tetradecane. The types of sulfur compounds can vary significantly. To further investigate the ODS performance of Ti-HHS-3, other sulfur compounds, specifically 4-MDBT and 4,6-DMDBT, were selected to evaluate their ODS performance with Ti-HHS-3 as the catalyst in model diesel. The experimental results (Figure 15) demonstrate that Ti-HHS-3 exhibits excellent catalytic activity in both short-chain alkanes (n-octane) and long-chain alkanes (n-tetradecane), with no significant difference in catalytic performance between the two alkanes. However, the presence of methyl groups in the molecular structure of 4-MDBT and 4,6-DMDBT introduces steric hindrance, limiting interaction between the reactive Ti sites on the catalyst and the sulfur compounds [51,52]. Consequently, the conversion rates for 4-MDBT and 4,6-DMDBT are lower than that of DBT at the 2 min, 5 min, and 10 min mark, highlighting the impact of molecular structure on ODS efficiency and providing valuable insights for the desulfurization of diesel oils.

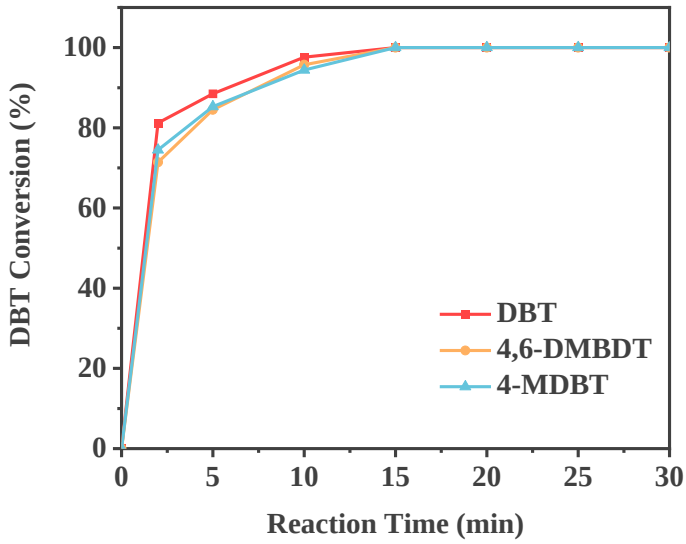

Figure 15. Conversion of different sulfur compounds in model diesel (reaction conditions: 20 g of 500 ppm model oil, 20 mg catalyst, O/S = 3).

In addition to the factors mentioned above, the effect of stirring speed on the ODS reaction should also be examined (as shown in Figure 16). For consistency, the stirring speed was maintained at 300 r/min in other experiments. The results show that the catalytic activity of the ODS reaction remained largely unaffected by changes in stirring speed. Specifically, whether the stirring speed is set at 300 r/min or adjusted to 100 r/min or 500 r/min, the ODS reaction proceeds similarly. This indicates that, under the experimental conditions used, stirring speed only slightly impacts on the catalytic activity of the ODS reaction.

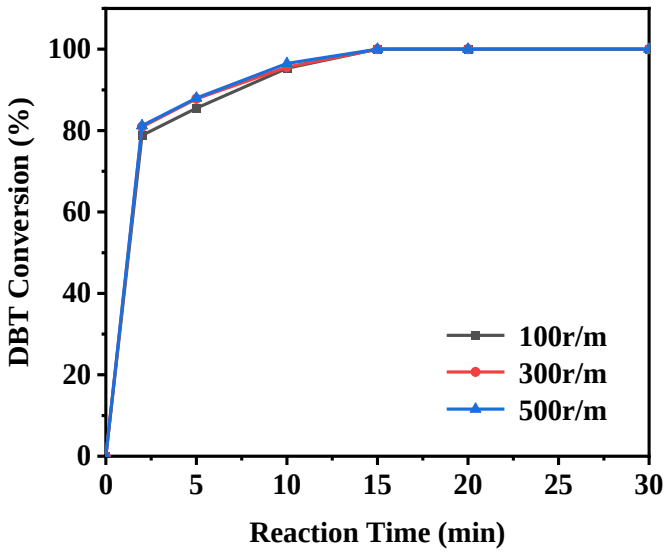

Figure 16. Effect of stirring speed on DBT conversion (reaction conditions: 20 g of 500 ppm model gasoline, 20 mg catalyst, O/S = 3).

In previous research [46], the ODS reaction typically involves the decomposition of the oxidant on the catalyst surface, producing active radicals. Electron paramagnetic resonance (EPR) characterization is conducted to confirm the generation of active radicals within the Ti-HHS-3 catalytic system. By using 5,5-dimethyl-1-pyrroline-N-oxide

(DMPO) as a radical trap at room temperature, the addition of the oxidant TBHP resulted in a typical radical/DMPO adduct signal (Figure 17). Based on the literature [53], the average spacing of the four stable peaks with a height ratio of 1:2:2:1 is 14.9 Gs, which indicates hydroxyl radicals were produced in the catalytic system. Hydroxyl radicals, as highly reactive species, can effectively oxidize DBT, thus facilitating desulfurization. The EPR spectrum confirms hydroxyl radical production during Ti-HHS-3 catalyzes DBT oxidation, supporting a radical-based oxidation mechanism for the ODS reaction.

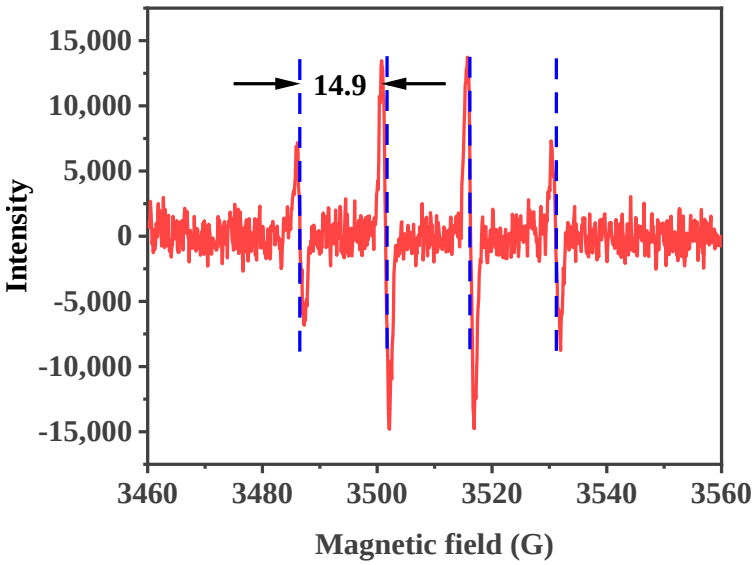

Figure 17. EPR spectrum of Ti−HHS−3. (The red lines indicate the EPR signals and the blue lines demonstrate the spacing of the signal peaks.).

3. Materials and Methods

3.1. Materials

Cetyltrimethylammonium bromide (CTAB, 99%), tetraethyl orthosilicate (TEOS, ≥99%), tetrabutyl titanate (TEOT, 99%), ammonium hydroxide (25–28 wt%), dibenzothiophene (DBT, ≥99 wt%), 4-methyl dibenzothiophene (4-MDBT, ≥99 wt%), 4,6-dimethyl dibenzothiophene (4,6-DMDBT, ≥99 wt%), n-octane (≥99 wt%), and n-tetradecane (≥99 wt%) were purchased from Aladdin Biochemical Technology (Shanghai, China). Anhydrous ethanol (≥99 wt%) was obtained from Tianjin Bohua Chemical Reagent (Tianjin, China). Tert-butyl hydroperoxide (TBHP, 5.0–6.0 mol/L in decane) was acquired from Sigma-Aldrich (Shanghai, China). Tetrapropylammonium hydroxide (TPAOH, 25 wt%) was purchased from Meryer Chemical Technology (Shanghai, China), and polyacrylic acid (PAA, 25 wt%, MW = 240,000) was obtained from Thermo Fisher Scientific (Shanghai, China).

3.2. Synthesis of Ti-HHS

To prepare the HHS precursor solution, mix 6 mL of TPAOH solution with 12 mL of deionized water and stir for 15 min until homogeneous. Then, add 5.6 mL of TEOS and a specified amount of TEOT (0.075 mL, 0.15 mL, and 0.3 mL) to achieve Si/Ti molar ratios of 116, 58, and 29, respectively. Continue stirring for 2 h to allow the hydrolysis of Si and Ti sources, resulting in a clear solution. Place the solution in a sealed container and let it stand at 45 °C for 3 days; the resulting clear solution is the HHS precursor solution. Here, the transparent solution containing zeolite structural units was prepared as the precursor for hierarchically porous titanosilicate hollow spheres (HHS).

Dissolve 0.56 g of CTAB in 20 mL of deionized water, stirring at 60 °C until CTAB is fully dissolved. After the solution becomes clear, bring the solution to room temperature, then add 3.0 g of PAA, and stir for 20 min until the solution is clear again. While stirring, add 2.0 g of ammonium hydroxide, which will immediately turn the solution milky white; continue stirring for another 20 min. Then, add 8.8 mL of precursor solution with varying Si/Ti molar ratios and stir at room temperature for 2 h. Transfer the emulsion to a 50 mL autoclave and let it stand at 80 °C for 2 days. Collect the product by centrifugation, wash it twice with deionized water and anhydrous ethanol, and dry it at 60 °C for 12 h. Calcine at 550 °C for 6 h to remove the template. Samples with varying Ti contents, obtained by adding 0.075 mL, 0.15 mL, and 0.3 mL of the Ti source, are designated as Ti-HHS-1, Ti-HHS-2, and Ti-HHS-3, respectively. When 0 mL of TEOT is added and the other synthesis steps are as above, a pure silicon hollow (HHS) sphere sample is obtained. A surfactant-polymer composite was used as the structure-directing agent, which became colloidal particles via self-assembly between anionic PAA and cationic CTAB. Under alkaline conditions, a series of Ti-HHS catalysts with varying titanium contents (Ti-HHS-1, Ti-HHS-2, and Ti-HHS-3) were successfully synthesized. The HHS precursor, with its larger volume and greater polymerization capability compared to monomeric or oligomeric silicates, is unable to penetrate the interior of the PAA-CTAB template. Consequently, co-assembly of the silicon source with the template and phase separation of PAA primarily occur at the surface of the PAA-CTAB composite, resulting in the formation of a thin shell. During calcination, the template is removed, leaving behind a hollow spherical structure.

For preparation of TiO_2-supported samples, a certain amount of tetrabutyl titanate was dissolved in 1 mL of deionized water, 0.1 g of pure silica hollow spheres was added to the above solution after continuous stirring for 2 h at room temperature, and then it was put into a vacuum oven and dried at 40 °C for 10 h. The solid samples were taken and ground and then roasted at 400 °C for 2 h in air, which yielded TiO_2/HHS-1 and TiO_2/HHS-2, with Si/Ti ratios of 58 and 29, respectively.

3.3. Characterization

X-ray diffraction (XRD) patterns were recorded on a Rigaku Smart Lab 3 kW instrument (Tokyo, Japan) using Cu Kα radiation (40 kV, 40 mA). Wide-angle diffraction patterns were measured in the 2θ range of 5–50° with a scan speed of 8° per minute, while small-angle diffraction patterns were measured in the 2θ range of 1–5° with a scan speed of 0.1° per minute. Scanning electron microscopy (SEM) images were taken using a JSM-7800F (JEOL, Tokyo, Japan). The SEM instrument operates under vacuum conditions, and samples were gold-sputtered prior to testing. Transmission electron microscopy (TEM) images were obtained with a JEM-2800 (JEOL, Japan). Nitrogen adsorption–desorption isotherms were obtained using a JW-TB220A analyzer from JWGB Sci & Tech Co., Ltd. (Beijing, China). Samples were pretreated at 350 °C under nitrogen flow for 4 h prior to measurement. The specific surface area was calculated using the Brunauer–Emmett–Teller (BET) model (JWGB, Beijing, China); the microporous pore volume (V_{mic}) and the mesoporous pore volume (V_{mes}) were obtained by DFT method. Infrared spectra were collected on a Bruker VECTOR 22 spectrometer (Billerica, USA), with samples prepared by pressing into KBr pellets; the position and shape of absorption peaks were analyzed to characterize whether Si-O-Ti structures were present in the silicate materials. The diffuse reflectance UV–visible (UV-vis) spectra of the dehydrated samples relative to $BaSO_4$ were measured using a Shimadzu (UV-2450) spectrophotometer (Tokyo, Japan) over a wavelength range of 500–2000 nm at room temperature. Electron paramagnetic resonance (EPR) spectra were recorded at room temperature using a Bruker EMX-plus X-band spectrometer

(Billerica, USA). Ti content was determined by inductively coupled plasma emission spectrometry (ICP) on a Thermo Scientific iCAP 7400 (Waltham, USA) atomic emission spectrometer.

3.4. Catalytic Tests

Dissolve 0.1 g DBT, 4,6-DMDBT, or 4-MDBT in 199.9 g of n-octane or n-tetradecane, stirring for 10 min, then seal and store as 500 ppm model gasoline. Place 20 g of model gasoline in a 50 mL Erlenmeyer flask and transfer it to a 30 °C water bath, stirring until the temperature stabilizes. Add 20 mg of the calcined hierarchically porous titanosilica hollow spheres as the catalyst and stir for another 10 min. Subsequently, add a specific amount of tert-butyl hydroperoxide (TBHP, 5.5 M in decane) solution to the system according to the predetermined oxygen-to-sulfur ratio. Start timing as soon as the oxidant is added. The stirring speed is maintained as 300 r/min. Samples are collected at various reaction times, and the catalyst is removed by filtering through a syringe with a membrane filter before analyzing reactant concentrations using a gas chromatograph (GC-7800, Grockway, Tengzhou, China). The signal detection during the analysis is performed using a flame ionization detector (FID). All catalysts were dehydrated at 150 °C for 2 h prior to use. The major ODS reaction conditions are listed in Table 3.

Table 3. The conditions for ODS reactions.

ODS Reaction Runs	Raw Material: Catalyst Ratio	Raw Material: Oxidant Ratio	O/S Ratio	Temperature (°C)	S Content (ppm)	Stirring Speed (r/min)
1	1000	1363	3	30	500	300
2	1000	4089	1	30	500	300
3	1000	454	9	30	500	300

3.5. Analysis

The GC-7800 equipped with a flame ionization detector (FID) was used to analyze the DBT, 4,6-DMDBT, and 4-MDBT concentration in the samples after the catalytic oxidation reaction, using high purity nitrogen as the carrier gas at a flow rate of 1 mL/min.

The conversion of DBT, 4,6-DMDBT, and 4-MDBT were calculated to evaluate the performance of the catalyst Ti-HHS. The reaction equation for oxidative desulfurization is based on the following equation:

$$\eta = [(C_0 - C)/C_0] \times 100\% \quad (1)$$

where η is the DBT, 4,6-DMDBT, and 4-MDBT conversion rate, and C_0 and C correspond to the initial and final concentration of DBT in model gasoline, respectively (Units: ppm).

The oxidant/sulfur molar ratio (O/S) of the reaction was evaluated using the following equation:

$$\alpha = n_o/n_s \quad (2)$$

where α is the O/S, and n_o and n_s denote the molar mass of oxidant added to the ODS and the molar mass of sulfur compound in the model gasoline, respectively.

4. Conclusions

In summary, a zeolite TS-1 precursor was successfully used as the source of Ti and Si, with a PAA-CTAB composite serving as the template, to synthesize hierarchically porous hollow spheres, Ti-HHS-x, under mildly alkaline conditions. The Ti-HHS-3 sample, with the highest Ti content, exhibited remarkable catalytic activity in the ODS reaction at room temperature. Using only 20 mg of catalyst, a complete conversion of DBT in 20 g of

500 ppm model gasoline was achieved at 30 °C with a TOF as high as 123 h^{-1}. This outstanding catalytic performance can be attributed to the tetrahedral coordination Ti of TS-1 sub-units and the hierarchically porous hollow structure of the material itself.

Author Contributions: Experiments, Y.W. and H.Y.; data analysis, Y.W., H.Y., and H.W.; writing—review and editing, funding acquisition and supervision, T.C. All authors have read and agreed to the published version of the manuscript.

Funding: This research received no external funding.

Data Availability Statement: The original contributions presented in this study are included in the article. Further inquiries can be directed to the corresponding author.

Conflicts of Interest: The authors declare no conflicts of interest.

References

1. Haruna, A.; Merican Aljunid Merican, Z.; Gani Musa, S.; Abubakar, S. Sulfur Removal Technologies from Fuel Oil for Safe and Sustainable Environment. *Fuel* **2022**, *329*, 125370.
2. Si, Y.; Jiang, F.; Qiang, L.; Teng, X.; Gong, C.; Tang, Q. A Visible-Light-Responsive Molecularly Imprinted Polyurethane for Specific Detection of Dibenzothiophene in Gasoline. *Anal. Methods* **2022**, *14*, 1254–1260.
3. Song, C.; Ma, X. New Design Approaches to Ultra-Clean Diesel Fuels by Deep Desulfurization and Deep Dearomatization. *Appl. Catal. B Environ.* **2003**, *41*, 207–238.
4. Gao, S.; Yu, G.; Abro, R.; Abdeltawab, A.A.; Al-Deyab, S.S.; Chen, X. Desulfurization of Fuel Oils: Mutual Solubility of Ionic Liquids and Fuel Oil. *Fuel* **2016**, *173*, 164–171.
5. Jiang, Z.; Lü, H.; Zhang, Y.; Li, C. Oxidative Desulfurization of Fuel Oils. *Chin. J. Catal.* **2011**, *32*, 707–715.
6. Khalid, H.; Umar, A.; Saeed, M.H.; Nazir, M.S.; Akhtar, T.; Ikhlaq, A.; Ali, Z.; Hassan, S.U. Advances in Fuel Oil Desulfurization: A Comprehensive Review of Polyoxometalate Catalysts. *J. Ind. Eng. Chem.* **2024**, *141*, 32–45.
7. Pham, D.D.; Nguyen, T.M.; Ho, T.H.; Le, Q.V.; Nguyen, D.L.T. Advancing Hydrodesulfurization in Heavy Oil: Recent Developments, Challenges, and Future Prospects. *Fuel* **2024**, *372*, 132082.
8. Javadli, R.; de Klerk, A. Desulfurization of Heavy Oil. *Appl. Petrochem. Res.* **2012**, *1*, 3–19.
9. Kabir, S.F.; Zheng, R.; Delgado, A.G.; Fini, E.H. Use of Microbially Desulfurized Rubber to Produce Sustainable Rubberized Bitumen. *Resour. Conserv. Recycl.* **2021**, *164*, 105144.
10. Liu, Y.; Wang, H.; Zhao, J.; Liu, Y.; Liu, C. Ultra-Deep Desulfurization by Reactive Adsorption Desulfurization on Copper-Based Catalysts. *J. Energy Chem.* **2019**, *29*, 8–16.
11. Mahmood, Q.A.; Humadi, J.I.; Algawi, R.J.; Nawaf, A.T.; Ahmed, I.A. Adsorption Desulfurization of Simulated Diesel Fuel Using Graphene Oxide. *Chem. Chem. Technol.* **2024**, *18*, 436–441.
12. Kianpour, E.; Azizian, S.; Yarie, M.; Zolfigol, M.A.; Bayat, M. A Task-Specific Phosphonium Ionic Liquid as an Efficient Extractant for Green Desulfurization of Liquid Fuel: An Experimental and Computational Study. *Chem. Eng. J.* **2016**, *295*, 500–508.
13. Wang, P.; Jiang, L.; Zou, X.; Tan, H.; Zhang, P.; Li, J.; Liu, B.; Zhu, G. Confining Polyoxometalate Clusters into Porous Aromatic Framework Materials for Catalytic Desulfurization of Dibenzothiophene. *ACS Appl. Mater. Interfaces* **2020**, *12*, 25910–25919.
14. Pyshyev, S.; Korchak, B.; Miroshnichenko, D.; Vytrykush, N. Influence of Water on Noncatalytic Oxidative Desulfurization of High-Sulfur Straight-Run Oil Fractions. *ACS Omega* **2022**, *7*, 26495–26503.
15. Sahraei, S. Assessment of Reaction Parameters in the Oxidative Desulfurization Reaction. *Energy Fuels* **2023**, *37*, 15373–15393.
16. Ma, C.; Dai, B.; Liu, P.; Zhou, N.; Shi, A.; Ban, L.; Chen, H. Deep Oxidative Desulfurization of Model Fuel Using Ozone Generated by Dielectric Barrier Discharge Plasma Combined with Ionic Liquid Extraction. *J. Ind. Eng. Chem.* **2014**, *20*, 2769–2774.
17. Mirshafiee, F.; Movahedirad, S.; Sobati, M.A.; Alaee, R.; Zarei, S.; Sargazi, H. Current Status and Future Prospects of Oxidative Desulfurization of Naphtha: A Review. *Process Saf. Environ. Prot.* **2023**, *170*, 54–75.
18. García-Gutiérrez, J.L.; Laredo, G.C.; García-Gutiérrez, P.; Jiménez-Cruz, F. Oxidative Desulfurization of Diesel Using Promising Heterogeneous Tungsten Catalysts and Hydrogen Peroxide. *Fuel* **2014**, *138*, 118–125.
19. Chica, A.; Corma, A.; Dómine, M.E. Catalytic Oxidative Desulfurization (Ods) of Diesel Fuel on a Continuous Fixed-Bed Reactor. *J. Catal.* **2006**, *242*, 299–308.
20. Tang, Q.; Lin, S.; Cheng, Y.; Liu, S.; Xiong, J.-R. Ultrasound-Assisted Oxidative Desulfurization of Bunker-C Oil Using Tert-Butyl Hydroperoxide. *Ultrason. Sonochem.* **2013**, *20*, 1168–1175.

21. Ding, Y.; Wang, J.; Liao, M.; Li, J.; Zhang, L.; Guo, J.; Wu, H. Deep Oxidative Desulfurization of Dibenzothiophene by Novel Pom-Based Il Immobilized on Well-Ordered Kit-6. *Chem. Eng. J.* **2021**, *418*, 129470.
22. Bakar, W.A.W.A.; Ali, R.; Kadir, A.A.A.; Mokhtar, W.N.A.W. Effect of Transition Metal Oxides Catalysts on Oxidative Desulfurization of Model Diesel. *Fuel Process. Technol.* **2012**, *101*, 78–84.
23. Caero, L.C.; Hernández, E.; Pedraza, F.; Murrieta, F. Oxidative Desulfurization of Synthetic Diesel Using Supported Catalysts: Part I. Study of the Operation Conditions with a Vanadium Oxide Based Catalyst. *Catal. Today* **2005**, *107–108*, 564–569.
24. Du, Q.; Guo, Y.; Wu, P.; Liu, H.; Chen, Y. Facile Synthesis of Hierarchical Ts-1 Zeolite without Using Mesopore Templates and Its Application in Deep Oxidative Desulfurization. *Microporous Mesoporous Mater.* **2019**, *275*, 61–68.
25. Lv, G.; Deng, S.; Zhai, Y.; Zhu, Y.; Li, H.; Wang, F.; Zhang, X. P123 Lamellar Micelle-Assisted Construction of Hierarchical Ts-1 Stacked Nanoplates with Constrained Mesopores for Enhanced Oxidative Desulfurization. *Appl. Catal. A Gen.* **2018**, *567*, 28–35.
26. Wang, H.; Shi, C.; Chen, S.; Chen, R.; Sun, P.; Chen, T. Hierarchically Mesoporous Titanosilicate Single-Crystalline Nanospheres for Room Temperature Oxidative–Adsorptive Desulfurization. *ACS Appl. Nano Mater.* **2019**, *2*, 6602–6610.
27. Wang, J.; Wu, W.; Ye, H.; Zhao, Y.; Wang, W.-H.; Bao, M. Moo3 Subnanoclusters on Ultrasmall Mesoporous Silica Nanoparticles: An Efficient Catalyst for Oxidative Desulfurization. *RSC Adv.* **2017**, *7*, 44827–44833.
28. Cho, K.-S.; Lee, Y.-K. Effects of Nitrogen Compounds, Aromatics, and Aprotic Solvents on the Oxidative Desulfurization (Ods) of Light Cycle Oil over Ti-Sba-15 Catalyst. *Appl. Catal. B Environ.* **2014**, *147*, 35–42.
29. Hao, L.; Sun, L.; Su, T.; Hao, D.; Liao, W.; Deng, C.; Ren, W.; Zhang, Y.; Lü, H. Polyoxometalate-Based Ionic Liquid Catalyst with Unprecedented Activity and Selectivity for Oxidative Desulfurization of Diesel in [Omim]Bf4. *Chem. Eng. J.* **2019**, *358*, 419–426.
30. Hori, H.; Ogi, K.; Fujita, Y.; Yasuda, Y.; Nagashima, E.; Matsuki, Y.; Nomiya, K. Oxidative Removal of Dibenzothiophene and Related Sulfur Compounds from Fuel Oils under Pressurized Oxygen at Room Temperature with Hydrogen Peroxide and a Phosphorus-Free Catalyst: Sodium Decatungstate. *Fuel Process. Technol.* **2018**, *179*, 175–183.
31. Ramaswamy, V.; Shah, P.; Lazar, K.; Ramaswamy, A.V. Synthesis, Characterization and Catalytic Activity of Sn-Sba-15 Mesoporous Molecular Sieves. *Catal. Surv. Asia* **2008**, *12*, 283–309.
32. Han, Y.; Xiao, F.-S.; Wu, S.; Sun, Y.; Meng, X.; Li, D.; Lin, S.; Deng, F.; Ai, X. A Novel Method for Incorporation of Heteroatoms into the Framework of Ordered Mesoporous Silica Materials Synthesized in Strong Acidic Media. *J. Phys. Chem. B* **2001**, *105*, 7963–7966.
33. Wei, J.; Yue, Q.; Sun, Z.; Deng, Y.; Zhao, D. Synthesis of Dual-Mesoporous Silica Using Non-Ionic Diblock Copolymer and Cationic Surfactant as Co-Templates. *Angew. Chem. Int. Ed.* **2012**, *51*, 6149–6153.
34. Chen, D.; Li, Z.; Yu, C.; Shi, Y.; Zhang, Z.; Tu, B.; Zhao, D. Nonionic Block Copolymer and Anionic Mixed Surfactants Directed Synthesis of Highly Ordered Mesoporous Silica with Bicontinuous Cubic Structure. *Chem. Mater.* **2005**, *17*, 3228–3234.
35. Wang, J.-G.; Zhou, H.-J.; Sun, P.-C.; Ding, D.-T.; Chen, T.-H. Hollow Carved Single-Crystal Mesoporous Silica Templated by Mesomorphous Polyelectrolyte−Surfactant Complexes. *Chem. Mater.* **2010**, *22*, 3829–3831.
36. Gopalakrishnan, A.; Raju, T.D.; Badhulika, S. Green Synthesis of Nitrogen, Sulfur-Co-Doped Worm-Like Hierarchical Porous Carbon Derived from Ginger for Outstanding Supercapacitor Performance. *Carbon* **2020**, *168*, 209–219.
37. Li, Y.; Wu, Z.; Liu, Y.; Zhang, K.; Luo, S.; Li, W.; Liu, S. Worm-Like Ordered Mesoporous Carbon from Liquefied Wood: Morphological Manipulation by Varying Hydrothermal Temperature. *Aggregate* **2024**, *5*, e570.
38. Macina, D.; Opioła, A.; Rutkowska, M.; Basąg, S.; Piwowarska, Z.; Michalik, M.; Chmielarz, L. Mesoporous Silica Materials Modified with Aggregated Transition Metal Species (Cr, Fe and Cr-Fe) in the Role of Catalysts for Selective Catalytic Oxidation of Ammonia to Dinitrogen. *Mater. Chem. Phys.* **2017**, *187*, 60–71.
39. Ren, J.; Li, Z.; Liu, S.; Xing, Y.; Xie, K. Silica–Titania Mixed Oxides: Si–O–Ti Connectivity, Coordination of Titanium, and Surface Acidic Properties. *Catal. Lett.* **2008**, *124*, 185–194.
40. Liu, J.; Wang, J.; Zhang, Y.; Zheng, W.; Yao, Y.; Liu, Q.; Zhang, X.; Yang, Y.; Wang, X. Improved C–H Activation in Propane Dehydrogenation Using Zeolite-Stabilized Co–O Moieties. *ACS Catal.* **2023**, *13*, 14737–14745.
41. Liang, Z.; Yang, Y.; Zhang, Y.; Li, S.; Zhang, W.; Zhang, L.; Chan, S.H. Synergistic Photocatalysis of Mesoporous Confinement Effect and Si-O-Ti Interface for Organic Pollutants Degradation. *Surf. Interfaces* **2024**, *51*, 104715.
42. Bhaumik, A.; Tatsumi, T. Organically Modified Titanium-Rich Ti-Mcm-41, Efficient Catalysts for Epoxidation Reactions. *J. Catal.* **2000**, *189*, 31–39.
43. Capel-Sanchez, M.C.; Campos-Martin, J.M.; Fierro, J.L.G. Removal of Refractory Organosulfur Compounds Via Oxidation with Hydrogen Peroxide on Amorphous Ti/SiO_2 Catalysts. *Energy Environ. Sci.* **2010**, *3*, 328–333.

44. de la Peña O'Shea, V.A.; Capel-Sanchez, M.; Blanco-Brieva, G.; Campos-Martin, J.M.; Fierro, J.L.G. The Usefulness of Time-Dependent Density Functional Theory to Describe the Electronic Spectra of Ti-Containing Catalysts. *Angew. Chem.* **2003**, *115*, 6031–6034.
45. Su, J.; Xiong, G.; Zhou, J.; Liu, W.; Zhou, D.; Wang, G.; Wang, X.; Guo, H. Amorphous Ti Species in Titanium Silicalite-1: Structural Features, Chemical Properties, and Inactivation with Sulfosalt. *J. Catal.* **2012**, *288*, 1–7.
46. Leng, K.; Li, X.; Ye, G.; Du, Y.; Sun, Y.; Xu, W. Ti-Containing Hierarchical Beta with Highly Active Sites for Deep Desulfurization of Fuels under Mild Conditions. *Catal. Sci. Technol.* **2016**, *6*, 7615–7622.
47. Shi, C.; Wang, W.; Liu, N.; Xu, X.; Wang, D.; Zhang, M.; Sun, P.; Chen, T. Low Temperature Oxidative Desulfurization with Hierarchically Mesoporous Titaniumsilicate Ti-Sba-2 Single Crystals. *Chem. Commun.* **2015**, *51*, 11500–11503.
48. Fang, Y.; Hu, H. Mesoporous Ts-1: Nanocasting Synthesis with Cmk-3 as Template and Its Performance in Catalytic Oxidation of Aromatic Thiophene. *Catal. Commun.* **2007**, *8*, 817–820.
49. Hulea, V.; Fajula, F.; Bousquet, J. Mild Oxidation with H2o2 over Ti-Containing Molecular Sieves—A Very Efficient Method for Removing Aromatic Sulfur Compounds from Fuels. *J. Catal.* **2001**, *198*, 179–186.
50. Soobramoney, L.; Bala, M.D.; Friedrich, H.B. Coordination Chemistry of Co Complexes Containing Tridentate Sns Ligands and Their Application as Catalysts for the Oxidation of N-Octane. *Dalton Trans.* **2014**, *43*, 15968–15978.
51. Stanger, K.J.; Angelici, R.J. Silica-Catalyzed Tert-Butyl Hydroperoxide Oxidation of Dibenzothiophene and Its 4,6-Dimethyl Derivative: A Route to Low-Sulfur Petroleum Feedstocks. *Energy Fuels* **2006**, *20*, 1757–1760.
52. Serrano, D.P.; Sanz, R.; Pizarro, P.; Moreno, I.; Medina, S. Hierarchical Ts-1 Zeolite as an Efficient Catalyst for Oxidative Desulphurization of Hydrocarbon Fractions. *Appl. Catal. B Environ.* **2014**, *146*, 35–42.
53. Teng, Z.; Yang, H.; Zhang, Q.; Cai, W.; Lu, Y.-R.; Kato, K.; Zhang, Z.; Ding, J.; Sun, H.; Liu, S.; et al. Atomically Dispersed Low-Valent Au Boosts Photocatalytic Hydroxyl Radical Production. *Nat. Chem.* **2024**, *16*, 1250–1260.